



This is a repository copy of *Electromagnetic-thermal coupled modelling and analysis of inter-turn short-circuit faults of a permanent magnet alternator*.

White Rose Research Online URL for this paper:  
<http://eprints.whiterose.ac.uk/144657/>

Version: Published Version

---

**Proceedings Paper:**

Chen, L., Wang, J. [orcid.org/0000-0003-4870-3744](https://orcid.org/0000-0003-4870-3744) and Sun, Z. (2019) Electromagnetic-thermal coupled modelling and analysis of inter-turn short-circuit faults of a permanent magnet alternator. In: *The Journal of Engineering*. The 9th International Conference on Power Electronics, Machines and Drives (PEMD 2018), 17-19 Apr 2018, Liverpool, UK. Institution of Engineering and Technology .

<https://doi.org/10.1049/joe.2018.8053>

---

**Reuse**

This article is distributed under the terms of the Creative Commons Attribution-NonCommercial-NoDerivs (CC BY-NC-ND) licence. This licence only allows you to download this work and share it with others as long as you credit the authors, but you can't change the article in any way or use it commercially. More information and the full terms of the licence here: <https://creativecommons.org/licenses/>

**Takedown**

If you consider content in White Rose Research Online to be in breach of UK law, please notify us by emailing [eprints@whiterose.ac.uk](mailto:eprints@whiterose.ac.uk) including the URL of the record and the reason for the withdrawal request.



[eprints@whiterose.ac.uk](mailto:eprints@whiterose.ac.uk)  
<https://eprints.whiterose.ac.uk/>

# Electromagnetic-thermal coupled modelling and analysis of inter-turn short-circuit faults of a permanent magnet alternator

eISSN 2051-3305  
Received on 21st June 2018  
Accepted on 27th July 2018  
doi: 10.1049/joe.2018.8053  
www.ietdl.org

Liang Chen<sup>1</sup>, Jiabin Wang<sup>2</sup> ✉, Zhigang Sun<sup>3</sup>

<sup>1</sup>Control Techniques Dynamics Ltd, Andover, UK

<sup>2</sup>Department of Electronic and Electrical Engineering, the University of Sheffield, Sheffield, UK

<sup>3</sup>Rolls-Royce plc, Derby, UK

✉ E-mail: j.b.wang@sheffield.ac.uk

**Abstract:** This paper describes a computationally efficient model for predicting transient and steady-state behaviours of a permanent magnet alternator (PMA) connected to an asymmetric PWM rectifier and load in aerospace applications under healthy and fault conditions. The model is validated by finite element and circuit coupled co-simulation. The developed model is used to predict the PMA performance under fault conditions and to identify fault signatures that can be exploited for the development of fault detection techniques. The developed electric model is coupled to the thermal model to predict hotspot temperature of the winding under the worst case inter-turn short-circuit condition and to estimate the winding lifetime.

## 1 Introduction

Inter-turn short circuit, also known as turn fault, resulting from insulation breakdown under combined electrical, mechanical, and thermal stresses is one of the most common fault types in electrical machines [1, 2]. The resultant short circuit is usually very large because the impedance associated with a few short-circuit turns are very small, leading to excessive heat which further degrades the insulation between the windings and lamination, and eventually leading to complete failure. Hence, accurate thermal analysis considering all effects is important at design stage for predicting the temperature distribution and hotspot temperature under healthy as well as fault conditions.

Usually, losses obtained from electromagnetic (EM) model are simply fed to a lumped parameter (LP) thermal model [3–5] to obtain the temperature distribution. Copper loss variation with temperature can be accounted under the assumption that the machine currents and back electromotive force (EMF) are independent of temperature. Under a turn fault condition, however, the turn fault current may be significantly influenced by the impedance of the short-circuited path, and hence EM-thermal-coupled analysis is required. Very few existing papers have considered the directly coupled EM-thermal simulation because of the complexity and different time constants between two physical fields. Moreover, fewer have considered coupled EM-thermal simulations under fault conditions.

However, EM-thermal-coupled simulation is vital under fault conditions, especially when the current is not known and dependent on the EM field. The inter-turn short circuit is a typical example, where the turn fault current is determined by the EMF, resistance, and reactance of the faulted turns while the turn copper loss is dependent on the turn fault current and turn resistance. In addition, resistance changes linearly with temperature, and the reactance depends on the operating speed and the number of faulted turns. Hence, there are three possible cases that will influence the short-circuit current, depending on which component of the short-circuit loop impedance is dominant: (i) resistant limited, (ii) inductance limited, and (iii) both resistance and inductance limited.

This paper analyses the fault behaviour of a permanent magnet alternator (PMA) in aerospace application under healthy and inter-turn short-circuit conditions. A computationally efficient EM model of the PMA under turn fault conditions is established and coupled to the thermal model of the machine for estimating the

winding hotspot temperature and lifetime in the worst-case scenario.

## 2 Inter-turn short-circuit fault problem

The PMA under study has 27 stator teeth and nine pole-pairs. To provide a level of redundancy, two sets of independent three-phase winding are employed, and each occupies nine slots as shown in Fig. 1a. The two 3-phase windings are separated by unwound teeth at both ends that provide thermal and magnetic isolations. Each phase consists of three tooth wound coils with 150 turns connected in series. However, the coils next to the unwound teeth are magnetically different from other coils and, hence, the three-phase systems are unbalanced.

An asymmetrical three-phase power electronic converter as shown in Fig. 1b is used at the PMA output to regulate the rectifier output voltage which supplies to a nominal load 20Ω. The three active devices switch simultaneously at a constant frequency of 5 kHz, while the duty ratio is controlled by the voltage regulator. When all the three devices are switched on, the PMA output is effectively terminally short-circuited, and hence the PMA output power to the load is pulse-width modulated.

It is well known that the worst short-circuit failure is one-turn short circuit (SC) because it results in the largest fault current. However, since the fault current is also influenced by the mutual inductances of the short-circuit turns with the healthy turns and other phases, which are dependent on the location of the fault in different slots and the position of the fault in a slot, a number of possible fault locations and positions, as shown in Fig. 2, are analysed in order to identify the worst case. It can be shown that the turns close to the slot opening on the two sides of each set of phase windings, denoted as SC1 and SC5 as shown in Fig. 2, have the highest SC current. The following analysis will focus on inter-turn SC that occurs in SC1 as an illustration example.

Since the PM field cannot be switched-off in an event of inter-turn SC, it is essential that the PMA can survive for a sufficient long period in the worst-case scenario. Further, effective techniques for detecting any SC faults are also necessary for mitigating action or informed replacement.

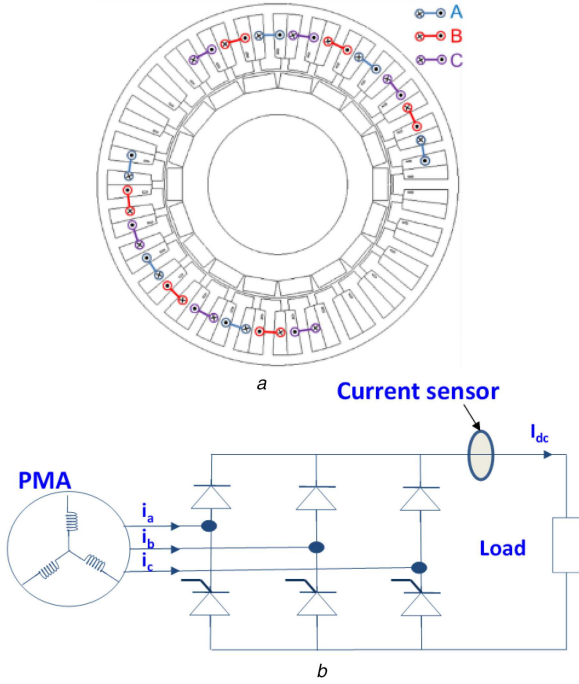


**Fig. 1** Schematic of (a) PMA, (b) its rectifier and load

### 3 High fidelity, computationally efficient modelling of inter-turn SC fault in PMA

The three-phase system of the PMA is unbalanced even in healthy conditions. The unconventional controlled rectifier operation coupled with a SC fault further increases the complexity of analysis and simulation study. It is possible to simulate the PMA operation in healthy and fault conditions by finite element analysis that is coupled to the controlled rectifier circuit and load. However, the process will be very time-consuming because a very small time step is required for the PWM operation. This simulation technique is, therefore, not practical for studying the PMA behaviour and for development of fault detection techniques. It is, therefore, essential to develop a high-fidelity, computationally model for the PMA power-generation system.

#### 3.1 Fault modelling

Without loss of generality, Fig. 3 shows the schematic coil connections of the PMA for one 3-phase channel. Each phase has three coils connected in series and an inter-turn SC fault is assumed in phase C. The third coil in phase C is separated into the healthy part  $c3_h$  and the faulty part  $c3_f$ . For the PMA with an inter-turn SC fault, the fault winding  $c3_f$  is also represented in addition to the three-phase windings  $a$ ,  $b$ , and  $c$ . As the two channels of the three-phase windings are electrically, magnetically, and thermally isolated, the analysis is focused on one channel of the three-phase windings whose governing equations are given in (1).  $V$ ,  $I$ ,  $\psi$  and  $R$  are the voltage, current, flux linkage, and resistance matrices for the windings with the SC turns.  $R_a$ ,  $R_b$ , and  $R_c$  are phase resistances. The ratio of the number of short-circuited turns,  $N_f$ , to the total number of series connected turns,  $N$ , in phase C is denoted as  $\mu = N_f/N$ . A short circuit may not be perfect, and this is represented by the fault resistance  $R_f$ .

The flux linkages of the four windings are magnetically coupled and vary with the phase currents and fault current, as well as rotor position due to the stator slotting effect. These relationships are expressed in (2) where the flux linkage of each winding is a four-variable function of phase currents  $i_a$ ,  $i_b$ , SC fault current  $i_f$  and rotor position  $\theta$  since in the star connection, phase C current  $i_c$  is not an independent variable. The phase currents  $i_a$  and  $i_b$  can be represented by their  $d$ - and  $q$ -axes components,  $i_d$ , and  $i_q$ . It is

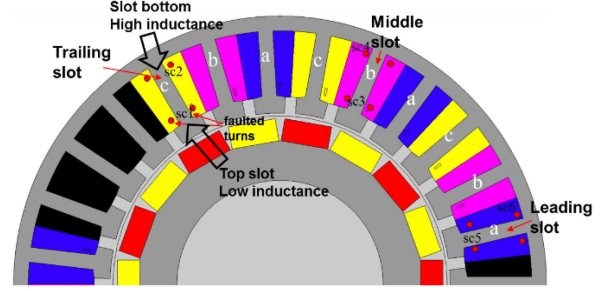


**Fig. 2** FE model of PMA with fault locations and positions studied

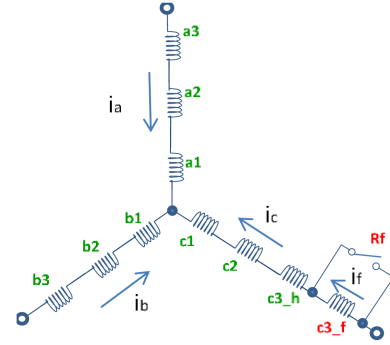


**Fig. 3** Three phase coils and SC coil in the machine model (assume fault in Phase C)

apparent that high-fidelity flux linkage functions are key to the modelling of the PMA machine.

The PMA FE model shown in Fig. 2 is utilised in building the flux linkage functions with current sources fed into the phase windings and faulty coils.

$$V = \frac{d\psi}{dt} + RI; \quad V = \begin{bmatrix} V_a \\ V_b \\ V_c \\ 0 \end{bmatrix}; \quad I = \begin{bmatrix} i_a \\ i_b \\ i_c \\ i_f \end{bmatrix} \quad (1)$$

$$\psi = \begin{bmatrix} \psi_a \\ \psi_b \\ \psi_c \\ \psi_f \end{bmatrix}; \quad R = \begin{bmatrix} R_a & 0 & 0 & 0 \\ 0 & R_b & 0 & 0 \\ 0 & 0 & R_c & -\mu R_c \\ 0 & 0 & \mu R_c & -(\mu R_c + R_f) \end{bmatrix}$$

$$\psi_i = g_i(i_a, i_b, i_f, \theta) = f_i(i_d, i_q, i_f, \theta) \quad (2)$$

$$i = a, b, c, f$$

At each given rotor position  $\theta$ , current sources  $i_a$ ,  $i_b$ ,  $i_c$ , and  $i_f$  are fed into the windings, respectively, and the flux linkages of the three-phase windings and the SC fault winding are computed by FE and recorded. With adequate current samples of  $(i_a, i_b, i_f)$  or  $(i_d, i_q, i_f)$  at various rotor position, four flux linkage tables, reflecting the iron core material non-linearity, each of which is of four dimensions, are built. Thus, flux linkages at a given  $(i_d, i_q, i_f, \theta)$  can be represented by four-dimensional look-up tables.

In order to save computation time on the look-up tables, at a given  $\theta$  and  $i_f$ , the flux linkage functions of  $(i_d, i_q)$  are curve-fitted into two-variable polynomial functions. Besides, since the number of short-circuited turns in the fault winding is relatively small compared to the total number of the turns in the phase, the fault current  $i_f$  has benign effect on the level of core saturation even if  $i_f$  is relatively larger. Thus, only two  $i_f$  samples are required in the FE calculations and the flux linkage variation with  $i_f$  is considered linear. By employing this technique, the four-dimensional flux linkage tables become only one-dimensional look-up tables for the polynomial coefficients with a single index  $\theta$ . Consequently, the model which can be used to represent healthy and fault behaviours of the PMA is both accurate and computationally efficient.

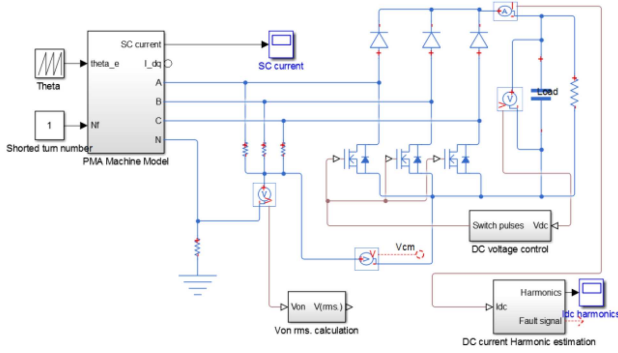


**Fig. 4** Simulation scheme in SimScape for PMA fault analysis and diagnosis

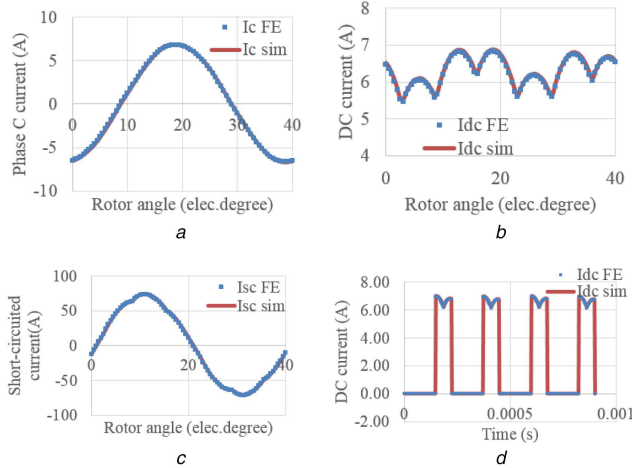


**Fig. 5** Comparison of FE and simulation model results at 15,000 rpm, uncontrolled rectifier with 20  $\Omega$  load for (a) Phase C current (healthy), (b) DC current (healthy), (c) SC current (1-turn SC) and controlled rectifier for, (d) DC current (healthy)

**Table 1** Comparison of rms currents in phase C and short-circuited turns predicted by SimScape and FE models at 15,000 rpm, rated load when the rectifier is uncontrolled

	FE (rms. A)	Sim (rms. A)	Difference, %
phase C current (Healthy)	4.82	4.86	0.805
phase C current (1-turn SC)	4.79	4.83	0.788
phase C current (4-turn SC)	4.74	4.77	0.578
SC current (1-turn SC)	56.6	56.97	0.648
SC current (4-turn SC)	31.8	32.03	0.738

As the magnetic field interaction between the fault winding and phase windings are dependent on relative positions where the fault occurs and also on the number of short-circuited turns  $N_f$ , it is necessary to build machine fault model for each possible fault position and number of short-circuited turns. In reality, the position where a SC fault occurs is unknown, and hence, a typical position that represents the worst case would be sufficient to study the fault behaviours.

The flux linkage maps are built with one-turn short circuit in phase C located close to the slot-opening, which represents the worst case in terms of the fault current. To represent an arbitrary number of short-circuited turns,  $N_f$ , the phase current,  $i_c$  and the fault current  $i_f$  should be adjusted by:

$$\begin{bmatrix} i_d \\ i_q \end{bmatrix} = T_p \begin{bmatrix} i_a \\ i_b \\ i_c \end{bmatrix}; \quad i_c' = \frac{N - N_f}{N - 1} i_c; \quad i_f' = N_f i_f \quad (3)$$

where  $T_p$  is the abc-to-dq transformation matrix, and the resultant flux-linkages are obtained by:

$$\psi_i = f_i(i_d, i_q, i_f, \theta), \quad i = a, b, c, f \quad (4)$$

It is possible that insulation breakdown results in a number of turns being short-circuited in parallel. Thus, for an  $n$ -parallel short-circuited turns at the same position, the machine fault model built under series inter-turn SC fault conditions is still applicable, but the effective number of shorted turn should be 1, and the shorted turn resistance should be  $1/n$  of the value of the 1-turn series SC fault model.

Fig. 4 shows the PMA simulation circuit established in Simulink–SimScape environment. The PMA model represented in (1) and (2) based on the flux linkages is connected to a controllable asymmetrical rectifier. The rectifier utilises three MOSFETs to control the PMA output power. When the rectifier is in the controlled mode, the DC voltage is fed back to the voltage control block in which the duty ratio of the three lower MOSFETs is pulse width modulated by a PI-controller so that the DC voltage is regulated close to the given reference. When the rectifier is in the uncontrolled mode, the MOSFETs are turned off and their body diodes act as a three-phase diode rectifier.

With the PMA simulation model, two inter-turn fault detection methods are studied. In the simulation scheme, the current harmonic estimation block receives the DC current measured through a current sensor and uses fast Fourier transform (FFT) or Kalman Filter to compute the amplitudes and frequencies of the harmonics contained in DC current which will be studied as the fault diagnostic signal. Also the zero-sequence voltage is monitored and its rms value is calculated as the other fault diagnostic signal.

### 3.2 Phase current and SC current

The simulation circuit with the PMA machine fault model is simulated under both healthy and various inter-turn SC fault conditions. The simulation results (denoted as ‘Sim’ thereafter) are compared with corresponding FE calculation results (denoted as ‘FE’) when the PMA operates at the max speed (15,000 rpm) with the rated load (20  $\Omega$ ), in the healthy or SC fault status, with the rectifier being controlled or uncontrolled, respectively. When a fault occurs, it is located in the worst fault position which is close to the slot opening at the trailing slot (Phase C) assuming  $R_f = 0$  as the worst case.

Figs. 5a and b compare FE and simulation model predicted phase C current waveforms and DC current waveforms, respectively, when the PMA operates in the healthy condition with uncontrolled rectifier. Fig. 5c compares currents in the SC fault turn when phase C has one turn short-circuited with uncontrolled rectifier while Fig. 5d compares the DC current with the controlled rectifier. The switch frequency is 5 kHz, and the MOSFET pulse width modulation ratio is fixed at 0.4 which means the on-state of the MOSFETs occupies 40% of a cycle. It can be seen that simulation results in the figures match quite very well with the FE predictions.

The quantitative validations of the model against FE predictions are performed when the PMA operates at 15,000 rpm, rated load, in the healthy status, 1-turn and 4-turn SC fault statuses and the rectifier is uncontrolled and the results are presented in Table 1, which compares rms currents in phase C and in faulted turns. It is shown that the relative differences between the two predictions are below 0.9% on the magnitude level  $\sim 5$  A. As will be shown in the following sections, for an inter-turn SC fault with a large number of turns per phase but a small number of short-circuited turns, the benign SC fault signature in the DC current component can be as low as 0.5% of 10 A magnitude level which is set as the minimum detectable fault signal. It follows that the high-fidelity PMA model is crucial for the inter-turn SC fault analyses and detection.

When the rectifier is uncontrolled, Fig. 6 shows the variations of phase rms current and SC rms current with the number of SC turns. It can be seen that when an inter-turn SC fault occurs, the phase current (healthy part) maintains the same magnitude level,

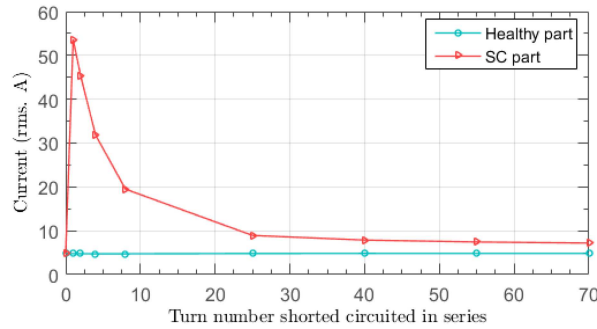


**Fig. 6** Rms current variations of healthy and fault parts with number of SC turns

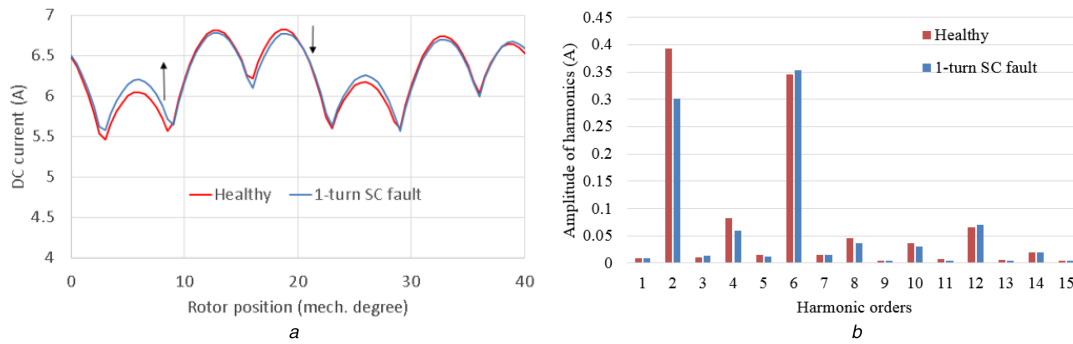


**Fig. 7** Comparison of DC output current under healthy and 1-turn SC conditions of (a) Waveform, (b) Harmonic components

**Table 2** Comparison of DC current harmonic spectrum predicted by SimScape and FE model at 15,000 rpm, rated load when the rectifier is uncontrolled

Harmonic orders	Healthy		1-turn SC		4-turn SC	
	Amp. (A) (Sim)	Diff. (%)	Amp. (A) (Sim)	Diff. (%)	Amp. (A) (Sim)	Diff. (%)
0	6.312	0.71	6.320	0.71	6.324	0.69
2	0.393	0.82	0.301	0.79	0.203	0.65
4	0.083	0.26	0.060	0.12	0.034	0.22
6	0.345	0.51	0.353	0.69	0.355	0.51

but SC current (in the short-circuited turns) changes significantly. The worst case occurs at 1-turn SC fault when the SC current increases up to 12 times of the phase current and creates ~124 times higher local heat load than healthy operation. As the number of SC turns increases, the SC current decreases, approaching the normal phase current magnitude when the number of SC turns is >25.

#### 4 Inter-turn short-circuit fault detection

Under balanced operating conditions, the harmonics in the DC output current are of 6th order and its integer multiples. Since an inter-turn fault results in unbalanced operation, the second-order harmonic will appear. Thus, by monitoring the second-order harmonic in the DC output current, it is possible to detect the fault. However, the problem is compounded by the fact that the three-phase system of the PMA is inherently unbalanced due to the presence of unwound teeth. This is seen in the DC current at the healthy status shown in Fig. 7.

Figs. 7a and b compare the DC currents and their spectrum under the healthy and 1-turn fault conditions at 15,000 rpm with uncontrolled rectifier. As is evident, the difference caused by the fault in the DC current is quite small.

The accuracy of the proposed model on DC current harmonics prediction is examined. Table 2 compares the amplitudes of main harmonics in the DC current predicted by the PMA simulation model and FE model under the same conditions stated previously. The prediction differences of the model compared to the FE model are maintained under 0.9%.

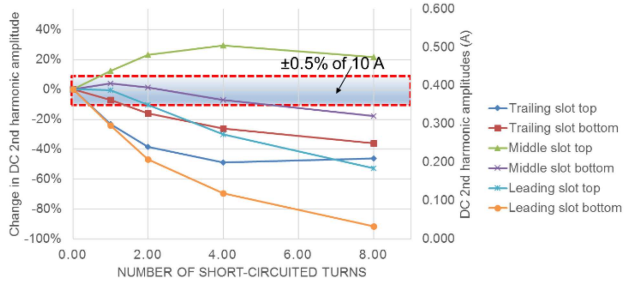
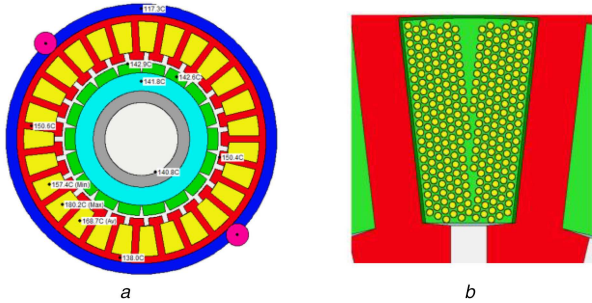
Table 3 lists the values of each harmonic amplitude under the healthy and fault conditions. It is seen from the harmonic spectrum

that the second-order harmonic is present alongside with other even harmonics. The change in the 6th harmonic due to fault is very little, while the change in the 2nd harmonic is more noticeable. Although the relative changes in the 4th and 10th harmonics appear to be large under the fault condition, their base values are an order of magnitude lower than that of the 2nd harmonic. It is, therefore, not possible to detect these changes with limited sensor resolution in an electrically noise environment. Monitoring the change in the 2nd harmonic, DC output current is the best option for the fault detection based on the DC current.

Fig. 8 compares the percentage changes in the 2nd harmonic currents under various fault locations and numbers of SC turns when the PMA operates uncontrolled at 15,000 rpm. The positive values indicate increases in the harmonic current, while the negative values indicate the reductions of the harmonic current due to the fault compared with the 2nd harmonic under the healthy condition. As can be seen, increase or decrease in the 2nd harmonic under a fault condition depends on the fault location in different slots. This is because the fault location affects the phase angle of the flux produced by the fault current, which in turn influences the phase unbalance that is reflected in the second harmonic current. It is also evident that the change in the 2nd harmonic current is very small if an SC fault with the number of short-circuited turns less than eight takes place in the middle slot closed to the back-iron. Assume that the dynamic range and accuracy of the current measurement are 0~4.0A and 0.5%, respectively, the absolute accuracy of the current measurement will be  $\pm 10$  mA. Since the 2nd harmonic current under healthy condition is in the region of 0.4A, the absolute current measurement accuracy corresponds to  $\pm 5\%$  change in the 2nd harmonic current. Therefore, if the change in the 2nd harmonic current due to a fault is below  $\pm 5\%$ , as

**Table 3** Comparison harmonic spectrum under healthy and fault conditions

Harmonic number	Healthy, A	1-turn fault, A	Relative change, %
2	0.390	0.299	-23.3
4	0.083	0.060	-28.0
6	0.343	0.351	2.2
8	0.045	0.036	-20.3
10	0.037	0.030	-18.7
12	0.065	0.070	7.4

**Fig. 8** Changes in 2nd harmonic current due to SC faults at 15,000 rpm**Fig. 9** PMA thermal model of (a) Whole machine for average temperature, (b) Slot FE model for local hotspot temperature

indicated in the shaded region inside the red-dotted box in Fig. 8, it is unlikely the fault can be detected. When a fault occurs in the leading or trailing slot closed to the slot opening compared to those in the other slots close to the back-iron, the fault signal is larger.

## 5 Electromagnetic-thermal-coupled modelling

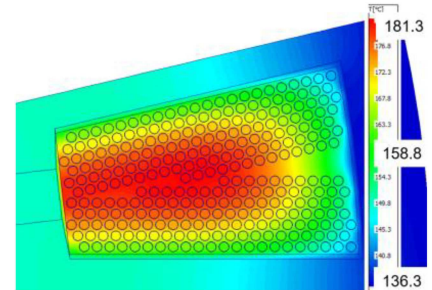
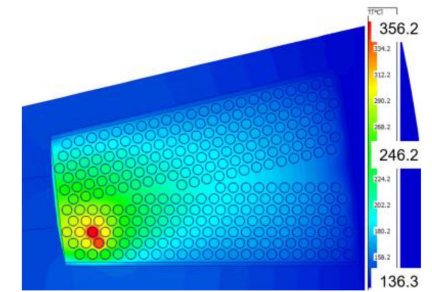
### 5.1 Thermal model

To assess the thermal behaviour of the PMA in SC fault conditions, a LP thermal model using Motor-CAD [6], Fig. 9a, is built to predict average temperatures of PMA components such as windings, magnets, and housing, and a slot FE model, Fig. 9b, is built to predict the local hot-spot temperature. The copper loss per turn is inputted to each turn in the slot FE model. When an inter-turn SC occurs, the copper loss of SC turns is calculated from the SC current of the PMA high-fidelity model described above, and then input to the SC turns. Initially, the PMA is assumed operating at 15,000 rpm and 20 ohm load in healthy condition, the winding slot hotspot temperature is below 180°C.

As shown in Fig. 10a, the slot hotspot temperature at healthy condition from the FE calculation is  $\sim 180^\circ\text{C}$ . When a 1-turn SC fault occurs which is the worst among inter-turn SC faults, the SC current is 12 times of phase current, resulting in the hotspot temperature risen significantly to 356°C.

### 5.2 Electro-thermal coupled method

In the previous discussions, the EM behaviours and thermal behaviours PMA under inter-turn SC faults are calculated separately. In fact, there is significant electro-thermal-coupling effect in the SC fault conditions: the high temperature in the SC turns caused by the SC current will increase the resistance greatly thus affecting the SC current rise. To consider the coupling effect,

**a****b****Fig. 10** Temperature distribution within a slot in (a) the healthy condition, (b) 1-turn short-circuit fault

the PMA EM model and the slot FE hotspot temperature simulation results are coupled together as shown in Fig. 11, where  $R_0$ ,  $T_{h0}$ ,  $E_0$  and  $P_{cu0}$  are the initial values at  $180^\circ\text{C}$  for the resistance, the hotspot temperature, the back-EMF caused by the magnets and the currents in phase windings, and the copper loss of the SC turns. The SC turn resistance is updated by the predicted hotspot temperature from FE thermal results, as in (5) where  $\alpha$  is the copper resistivity temperature coefficient. Since that the SC current has only marginal effect on the core saturation,  $E_0$  is considered as constant regardless of the SC current and  $T_h$ . Thus with updated resistance  $R(T_h)$  and reactance  $\omega L$ , the copper loss of the SC turns is updated by (6). Given that the temperature distribution predicted by the slot FE thermal model is linear with the copper loss distribution, the temperature rise  $\Delta T_h = T_h - 180$  from  $180^\circ\text{C}$  in the healthy condition is caused by the SC copper loss  $P_{cu}(T_h)$  and is proportional to  $P_{cu}(T_h)$ . Therefore, the hotspot temperature  $T_h$  is updated by (7). The newly obtained  $T_h$  is used in (5) again to update the resistance. The process shown in Fig. 11 proceeds iteratively until  $T_h$  finally converges.

$$R(T_h) = R_0[1 + \alpha(T_h - 154)] \quad (5)$$

$$P_{cu}(T_h) = E_0^2 \frac{R(T_h)}{R(T_h)^2 + (\omega L)^2} \quad (6)$$

$$T_h = \frac{P_{cu}(T_h)}{P_{cu0}}(T_{h0} - 180) + 180 \quad (7)$$

It should be noted that the method shown in Fig. 11 can also be used to directly couple the PMA EM model shown in Fig. 4, by importing the updated resistance from (5) to the EM model and

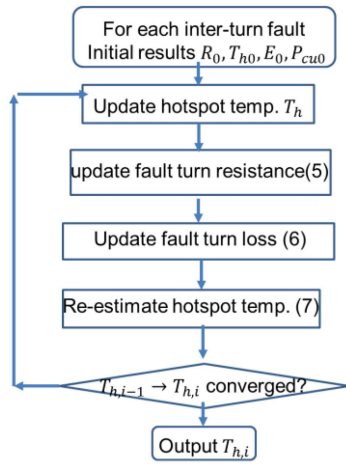


**Fig. 11** Flowchart for predicting hotspot temperature  $T_h$  in SC fault conditions

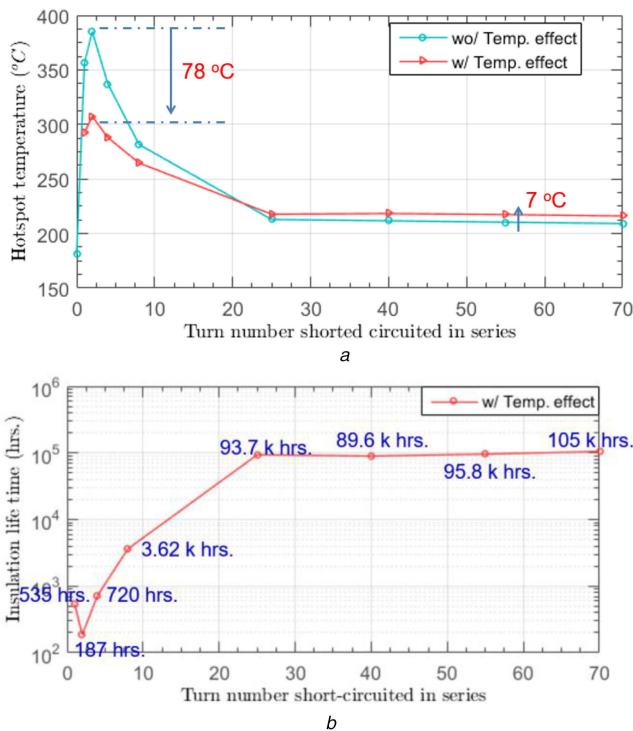


**Fig. 12** Electro-thermal simulation results of (a) Variation of hotspot temperature, (b) Variation of resultant insulation lifetime with number of SC turns

output the copper loss into the slot thermal equation in (7). Due to the limit of space, the process is not discussed here.

Fig. 12a shows the predicted hotspot temperatures for faults with different numbers of SC turns, using the electrothermal coupled method to consider the temperature effect on the resistance and SC current. Compared with the results without considering the temperature effect on the SC current, there are two different trends in the SC current and the temperatures. When a small number of turns are short-circuited, because the resistance effect is dominant in the short-circuited path, the high temperature reduces the SC current, and the steady-state hotspot temperature is lower than that when the coupling effect is not considered. If a large number of turns are short-circuited, the reactance effect becomes dominant, and the SC current is not affected by the temperature. As the resistance increases with temperature, the copper loss increases, and thus the steady-state hotspot temperature is higher than that when the coupling effect is neglected. It is seen from Fig. 12a that the highest temperature 307°C occurs when two turns are short-circuited rather than one turn is short-circuited. This is because two-turn SC current is close to that of one-turn SC, but its resistance is doubled, leading to higher copper loss.

Fig. 12b shows the predicted variation of the winding lifetime under SC faults with number of SC turns, assuming a typical lifetime of insulation is 20,000 h at 240°C (class R insulation) and it halves by every 10°C temperature rise. It can be seen that the lifetime is 535 h when a single turn is short-circuited. The lowest lifetime of 187 h occurs when two turns are short-circuited.

## 6 Conclusion

A high-fidelity, computationally efficient model for power generation system based on a dual channel PAM with asymmetrically controlled rectifier has been developed. The model can be coupled to the LP- and FE-based thermal models for predicting the hotspot temperatures in the SC turns. It has been shown that short circuit current in the worst case is ~12 times higher than rated, and the resultant hotspot temperature reaches 307°C. The lifetime of the windings is reduced to <187 h, albeit being sufficiently longer than any mission flight duration. The model is also used to analyse the fault signatures for development of a fault detection technique that can inform the need for replacement if a turn fault has occurred in a flight.

## 7 References

- [1] Sen, B.: 'Modelling, fault detection and control of fault tolerant permanent magnet machine drives'. PhD thesis, Univ. Sheff., September 2015
- [2] Sen, B., Wang, J.: 'Analytical modelling of stator turn fault in surface mounted permanent magnet machines'. 2013 IEEE Energy Convers. Congr. Expo. ECCE 2013, Denver, CO, USA, 2013, pp. 4445–4452
- [3] Wang, B., Wang, J., Griffio, A.: 'A fault tolerant machine drive based on permanent magnet assisted synchronous reluctance machine'. Proc. 2016 Energy Conversion Congress and Exposition (ECCE), MI, USA, 2016
- [4] Sarikhani, A., Mohammed, O.A.: 'Inter-turn fault detection in PM synchronous machines by physics-based back electromotive force estimation', *IEEE Trans. Ind. Electron.*, 2013, **60**, (8), pp. 3472–3484
- [5] Manana, M., Arroyo, A., Ortiz, A., *et al.*: 'Field winding fault diagnosis in DC motors during manufacturing using thermal monitoring', *Appl. Therm. Eng.*, 2011, **31**, (5), pp. 978–983
- [6] Motor Design Limited: 'Motor CAD user manual', 2016